Superfluid and Mott-insulator phases of one-dimensional Bose-Fermi mixtures

Zujev, A.; Baldwin, A.; Scalettar, R.T.; Rousseau, V.G.; Denteneer, P.J.H.; Rigol, M.

Superfluid and Mott-insulator phases of one-dimensional Bose-Fermi mixtures

A. Zujev, A. Baldwin, and R. T. Scalettar
Physics Department, University of California, Davis, California 95616, USA

V. G. Rousseau and P. J. H. Denteneer
Lorentz Institute, Leiden University, P.O. Box 9506, 2300 RA Leiden, The Netherlands

M. Rigol
Physics Department, University of California, Santa Cruz, California 95064, USA
and Department of Physics, Georgetown University, Washington, District of Columbia 20057, USA

We study the ground state phases of Bose-Fermi mixtures in one-dimensional optical lattices with quantum Monte Carlo simulations using the canonical worm algorithm. Depending on the filling of bosons and fermions, and the on-site intra- and interspecies interaction, different kinds of incompressible and superfluid phases appear. On the compressible side, correlations between bosons and fermions can lead to a distinctive behavior of the bosonic superfluid density and the fermionic stiffness, as well as of the equal-time Green functions, which allow one to identify regions where the two species exhibit anticorrelated flow. We present here complete phase diagrams for these systems at different fillings and as a function of the interaction parameters.

PACS number(s): 03.75.Mn, 05.30.Jp

I. INTRODUCTION

The experimental realization of strongly correlated systems with ultracold gases loaded in optical lattices [1] has generated tremendous excitement during recent years. Initially thought of as a way to simulate condensed matter model Hamiltonians, such as the Bose-Hubbard Hamiltonian [2], loading atoms on optical lattices has enabled the creation of quantum systems that are unexpected in the condensed matter context. Among these systems the realization of Bose-Fermi mixtures in optical lattices [3–5], where the inter- and intraspecies interactions can be tuned to be attractive or repulsive [6], is a remarkable example of the scope of realizable models.

Theoretical studies of Bose-Fermi mixtures in one-dimensional lattices have been done for homogeneous [7–13,17] and trapped [14–16] systems. Several approaches have been used: Gutzwiller mean-field theory [14], strong coupling expansions [8,17], bosonization [7,9], and exact analytical [10] and numerical [11–13,16,17] studies. Recently, a mixture of bosonic atoms and molecules on a lattice was studied numerically [18]. The landscape of phases encountered is expansive, and includes Mott insulators, spin and charge density waves, a variety of superfluids, phase separation, and Wigner crystals. However, the phase diagram in the chemical potential-interaction strength plane has not yet been reported.

It is our goal in this paper to present a study of repulsive Bose-Fermi mixtures in one-dimensional lattices that generalizes previous studies, which focused on specific special densities, to more general filling. After mapping the phase diagram we will explore different sections in greater detail. Since the particular case in which the lattice is half filled with bosons and half filled with fermions has been carefully studied in Ref. [11], we will instead concentrate here on two cases: (i) when the number of bosons is commensurate with the lattice size but the number of fermions is not, and (ii)

when the sum of both species is commensurate with the lattice size but the number of bosons and fermions are different. Some of the phases present in these cases have been identified by Sengupta and Pryadko in their grand canonical study in Ref. [12] and by Hébert *et al.* in the canonical study recently presented in Ref. [13].

The Hamiltonian of Bose-Fermi mixtures in one dimension can be written as

$$\hat{H} = -t_B \sum_l (b_{l+1}^\dagger b_l + b_l^\dagger b_{l+1}) - t_F \sum_l (f_{l+1}^\dagger f_l + f_l^\dagger f_{l+1})$$
$$+ U_{BB} \sum_l \hat{n}_l^B (\hat{n}_l^B - 1) + U_{BF} \sum_l \hat{n}_l^B \hat{n}_l^F, \quad (1)$$

where $b_l^\dagger (b_l)$ are the boson creation (destruction) operators on site l of the one-dimensional lattice with L sites. Similarly, $f_l^\dagger (f_l)$ are the creation (destruction) operators on site l for spinless fermions on the same lattice. For these creation and destruction operators $\hat{n}_l^{B,F}$ are the associated number operators. The bosonic and fermionic hopping parameters are denoted by t_B and t_F, respectively, and the on-site boson-boson and boson-fermion interactions by U_{BB} and U_{BF}. In this paper we will consider the case $t_B = t_F = 1$ (i.e., when the boson and fermion hopping integrals are equal) and choose $t_B = 1$ to set the scale of energy.

It is useful to begin a discussion of the phase diagram with an analysis of the zero hopping limit ($t_B = t_F = 0$) similar to the one done by Fisher *et al.* in Ref. [19] for the purely bosonic case. Consider a particular fermion occupation of one fourth of the lattice sites, $N_F = L/4$ fixed. Bosons can be added up to $N_B = 3L/4$ without sitting on a site which is already occupied by either a boson or a fermion. Therefore the associated chemical potential μ is small. What happens when N_B exceeds $3L/4$ depends on the relative strength of U_{BB} and U_{BF}.

If U_{BF} is less than $2U_{BB}$ then the extra bosons sit atop of the fermions and μ jumps by U_{BF}. The chemical potential stays at this elevated value of U_{BF} until all the sites with fermions also have a boson. At that point additional bosons start going onto sites with a boson already, and μ jumps to $2U_{BB}$. Thus, in general, there are incompressible phases where the boson chemical potential jumps both at commensurate $\rho_B = 1, 2, 3, \ldots$ (as for the pure boson-Hubbard model) and also at $\rho_B = 1 - \rho_F, 2 - \rho_F, 3 - \rho_F, \ldots$. For U_{BF} greater than $2U_{BB}$ and less than $6U_{BB}$ the incompressible phases still start at $\rho_B = 1 - \rho_F$ but the following potential jumps are shifted up by $1 - \rho_F$. Turning on the hoppings t_B, t_F introduces quantum fluctuations which will ultimately destroy these Mott plateaus and introduce new, intricate phases.

II. CANONICAL WORM ALGORITHM

We perform quantum Monte Carlo simulations (QMC) using a recently proposed canonical worm algorithm [20,21]. This approach makes use of global moves to update the configurations, samples the winding number, and gives access to the measurement of n-body Green functions. It also has the useful property of working in the *canonical* ensemble. This is particularly important for the present application since working with two species of particles leads to two different chemical potentials in the grand canonical ensemble. These prove difficult to adjust such that the precise, desired fillings are achieved. In our canonical simulations the Bose and Fermi occupations are exactly specified and the chemical potentials μ_B and μ_F are instead computed [22] via appropriate numerical derivatives of the resultant ground state energy [e.g., $\mu_B = E_0(N_B + 1) - E_0(N_B)$].

The canonical worm algorithm is a variation of the Prokof'ev *et al.* grand-canonical worm algorithm [23]. Within the canonical worm approach one starts by writing the Hamiltonian as $\hat{H} = \hat{V} - \hat{T}$, where $\hat{T}$ is comprised of the nondiagonal terms and is by necessity positive definite. The partition function $\mathcal{Z} = \mathrm{Tr}\, e^{-\beta \hat{H}}$ takes the form

$$\mathcal{Z} = \mathrm{Tr}\, e^{-\beta \hat{V}} \mathbf{T}_\tau e^{\int_0^\beta \hat{T}(\tau) d\tau} \tag{2}$$

$$= \mathrm{Tr}\, e^{-\beta \hat{V}} \sum_n \int_{0 < \tau_1 < \cdots < \tau_n < \beta} \hat{T}(\tau_n) \cdots \hat{T}(\tau_1) d\tau_1 \cdots d\tau_n, \tag{3}$$

where $\hat{T}(\tau) = e^{\tau \hat{V}} \hat{T} e^{-\tau \hat{V}}$. In order to sample expression (3) an extended partition function is considered by breaking up the propagator at imaginary time τ and introducing a "worm operator" $\hat{W} = \Sigma_{ijkl} w_{ijkl} b_i^\dagger b_j f_k^\dagger f_l$ that leads to $\mathcal{Z}(\tau) = \mathrm{Tr}\, e^{-(\beta - \tau)\hat{H}} \hat{W} e^{-\tau H}$. Complete sets of states are introduced between consecutive $\hat{T}$ operators to allow a mapping of the one-dimensional (1D) quantum problem onto a two-dimensional (2D) classical problem where a standard Monte Carlo technique can be applied. Measurements can be performed when configurations resulting in diagonal matrix elements of $\hat{W}$ occur. This way unphysical movements are exploited to help explore the Hilbert space, but are ignored when sampling for measurements.

As with pure bosonic systems, the evolution of the boson and fermion densities ρ_B, ρ_F with the associated chemical potential μ_B, μ_F identifies Mott-insulating behavior [19]. A jump in μ signals a Mott phase where the compressibility $\kappa_B = \partial \rho_B / \partial \mu_B$ or $\kappa_F = \partial \rho_F / \partial \mu_F$ vanishes.

Quantities of interest that we measure include the bosonic superfluid density and the fermionic stiffness,

$$\rho_B^s = \langle W_B^2 \rangle L/2\beta,$$

$$\rho_F^s = \langle W_F^2 \rangle L/2\beta. \tag{4}$$

Here $\langle W^2 \rangle$ are the associated winding numbers. Correlations between the bosonic and fermionic winding numbers [11] are determined by the combinations,

$$\rho_c^s = \langle (W_B + W_F)^2 \rangle L/2\beta,$$

$$\rho_a^s = \langle (W_B - W_F)^2 \rangle L/2\beta. \tag{5}$$

In addition to the usual bosonic and fermionic Green function,

$$G_{ij}^B = \langle b_i^\dagger b_j \rangle,$$

$$G_{ij}^F = \langle f_i^\dagger f_j \rangle, \tag{6}$$

we also measure the composite anticorrelated two-body Green function

$$G_{ij}^a = \langle b_i^\dagger b_j f_j^\dagger f_i \rangle. \tag{7}$$

In G_{ij}^a, the fermion and boson propagate in opposite directions (one from j to i and one from i to j).

The Fourier transforms of G_{ij}^B and G_{ij}^F give the densities $n_B(k)$ and $n_F(k)$ in momentum space; $n_a(k)$ is the Fourier transform of the composite two-body Green function G_{ij}^a.

We performed extensive checks of the code against other quantum Monte Carlo simulations in the pure boson and pure fermion cases, and against exact diagonalization and Lanczos calculations for mixed systems on small lattices.

III. PHASE DIAGRAM IN THE μ_B-U_{BF} PLANE

We begin our determination of the phase diagram by calculating the dependence of the density ρ_B on chemical potential μ_B, mapping out the extent that the Mott plateaus described in the Introduction survive the addition of quantum fluctuations t_B, t_F. We examine a system with a fixed $U_{BB} = 10$ and $\rho_F = 1/4$ and focus on the regions through $\rho_B \leq 3/2$ and $U_{BF} \leq 5U_{BB}/2$ in the phase diagram. The $t_B = t_F = 0$ analysis suggests for $U_{BF} < 2U_{BB}$ there will be plateaus with compressibility $\kappa = 0$ at $\rho_B + \rho_F = 1$ (i.e., $\rho_B = 3/4$) caused by U_{BF} and at $\rho_B = 1$ caused by U_{BB}. Figure 1 exhibits these plateaus for $U_{BF} = 16$ and $t_B = t_F = 1$. The complete phase diagram in the μ_B-U_{BF} plane at fixed $U_{BB} = 10$ is obtained by replicating Fig. 1 for different U_{BF}, and is given in Fig. 2(a). For weak U_{BF} the phase diagram is dominated by the $\rho_B = 1$ plateau where the chemical potential jumps by $2U_{BB} - U_{BF} \approx 2U_{BB} = 20$. As U_{BF} increases, this plateau shrinks and finally terminates at $U_{BF} \approx 2U_{BB} = 20$. At the same time, the
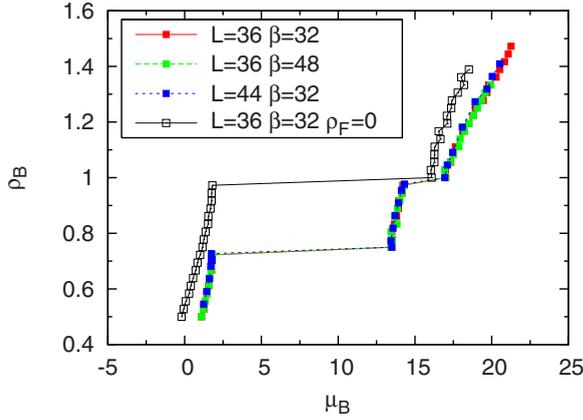
FIG. 1. (Color online) ρ_B as a function of chemical potential μ_B. The fermion density is $\rho_F = 1/4$ and the interaction strengths are fixed at $U_{BB} = 10$ and $U_{BF} = 16$. There are Mott plateaus at $\rho_B = 1 - \rho_F = 3/4$ and $\rho_B = 1$ as predicted by the $t_B = t_F = 0$ analysis. The positions of the Mott lobes coincide for different lattice sizes $L = 36, 44$ and temperatures $\beta = 32, 48$ to within our error bars, which are smaller than the symbol size. The dependence of ρ_B on μ_B in the absence of fermions is given for comparison.

plateau at $\rho_B = 1 - \rho_F$ grows to $U_{BF} = 20$. The explanation of the labeling of the different phases (I–VI) will be given after we discuss the superfluid response of the system. Figure 2(b) shows the phase diagram in the μ_B and U_{BB} plane.

IV. SUPERFLUID RESPONSE AT $\rho_B + \rho_F = 1$

After determining the positions of the Mott plateaus, we examine the stiffness and Green functions. We take a "horizontal" cut through Fig. 2(a) by fixing $\rho_B + \rho_F = 1$ ($\rho_B = 3/4$) and increasing U_{BF}. In Fig. 3 we see that for $U_{BF} \lesssim 2U_{BB} = 20$ the interaction strength U_{BF} is small enough that fermions and bosons can briefly inhabit the same site. Now, when a boson visits the site of a neighboring fermion (or vice versa) it is equally likely that the fermion will exchange as for the boson to return to its original site. Through these exchanges the bosons and fermions can achieve anticorrelated winding around the lattice. Thus, the bosonic superfluid density and the fermionic stiffness are both nonzero and identical [25]. However, as U_{BF} increases past $U_{BF} \approx 2U_{BB} = 20$ the cost of double occupancy becomes prohibitive. With its benefits outweighed by energy penalties exacted by U_{BF}, all anticorrelated "superfluidity" ceases. Pollet *et al.* [11] have argued that this region exhibits phase separation. Indeed we do detect a signal of phase separation through density structure factor. But the signal is weak, about 20 times weaker than what we get at phase VI (next section), and compressibility is close to zero, so we label this region as an insulator.

From the results depicted in Fig. 3 one should notice that while for quantities like the energy and Mott gap $\beta = 32$ is sufficiently low for $L = 32$ to capture the ground state behavior, for stiffnesses one requires much lower temperatures.

V. SUPERFLUID RESPONSE AT $\rho_B = 1$

Although it shares the property that $\kappa_B = 0$ with the $\rho_B + \rho_F = 1$ lobe, a horizontal cut (Fig. 4) through the $\rho_B = 1$ Mott
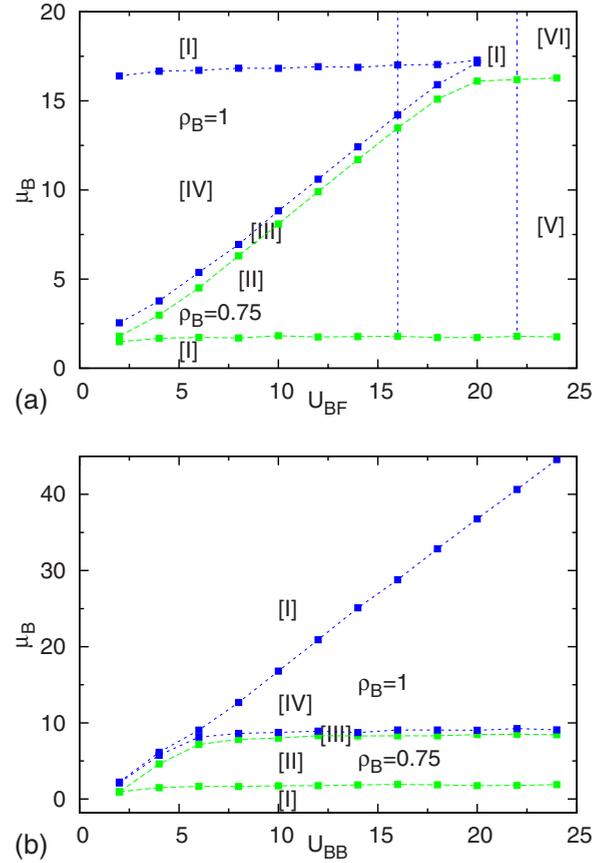

FIG. 2. (Color online) Top panel: Phase diagram in the μ_B-U_{BF} plane for $U_{BB} = 10$ and $\rho_F = 1/4$ obtained by a sequence of plots such as that in Fig. 1. The vertical line at $U_{BF} = 16$ corresponds to the coupling value in Fig. 1. Within the regions labeled $\rho_B = 0.75$ and $\rho_B = 1$, the boson density is frozen even though the chemical potential varies. The $\rho_B = 1$ lobe is pinched off at $U_{BF} \approx 2U_{BB}$. The labeling of the phases is I, superfluid ($\rho_B^s \neq 0$, $\rho_F^s \neq 0$); II, anticorrelated phase ($\rho_B^s \neq 0$, $\rho_F^s \neq 0$, $\rho_B^s = \rho_F^s$); III, anticorrelated phase/relay superfluid ($\rho_B^s \neq 0$, $\rho_F^s \neq 0$) (see the text for a detailed explanation); IV, Mott insulator/Luttinger liquid ($\rho_B^s = 0$, $\rho_F^s \neq 0$); V, insulator, $\rho_B^s = 0$, $\rho_F^s = 0$; VI, phase separation. Bottom panel: Phase diagram in the μ_B-U_{BB} plane for $U_{BF} = 10$ and $\rho_F = 1/4$. The upper boundary of phase II is defined by the increase of energy when a boson is added at filling $\rho_B + \rho_F = 1$; this is approximately $\mu_B = U_{BF}$ (for $U_{BF} < 2U_{BB}$), a line of slope 1 in the μ_B-U_{BF} plane and slope 0 in the μ_B-U_{BB} plane. A similar strong coupling analysis applies for the other boundaries. (See also Fig. 13 and [8].)

lobe exhibits rather different superfluid response. This trajectory initially lies within the Mott lobe and then emerges into a region of nonzero compressibilities. As expected, the plateau in ρ_B (Mott gap) indicates the bosons are locked into place by the strong U_{BB}, and as a consequence $\rho_B^s = 0$ (Fig. 4). Throughout this boson Mott lobe the fermions are, however, free to slide over the bosons and so ρ_F^s is nonzero. In this region, as expected, the fermion compressibility κ_F is nonzero.

The Bose-Fermi repulsion U_{BF} competes with U_{BB} and, in a window around $U_{BF} \approx 2U_{BB}$, it is energetically equivalent for a boson to share a site with another boson as with a fermion. The Mott lobe is terminated and a superfluid win-
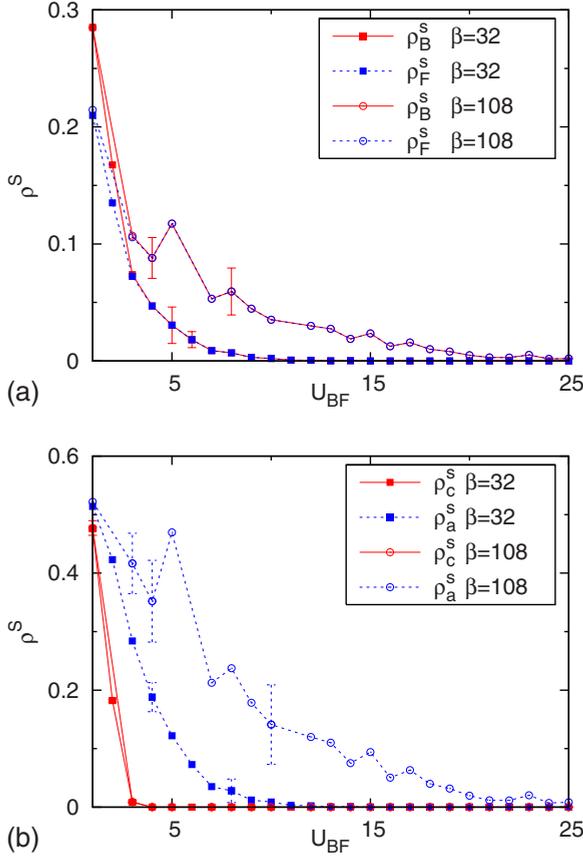
FIG. 3. (Color online) "Horizontal" sweep, which is fixed densities $\rho_B=3/4$ and $\rho_F=1/4$ and varying U_{BF}, through the phase diagram of Fig. 2. As in Figs. 1 and 2, $U_{BB}=10$. Top panel: Both the bosonic and fermionic species exhibit a finite stiffness at weak coupling (region II of the phase diagram), which decays as U_{BF} increases until insulating behavior occurs (region V of the phase diagram). Bottom panel: Near $U_{BF}=0$ both $\rho_c^s \neq 0$ and $\rho_a^s \neq 0$ are very similar. However, quickly after turning on U_{BF}, the correlated and anticorrelated stiffness show that the bosons and fermions propagate in opposite directions $\rho_a^s \neq 0$, while $\rho_c^s=0$.

FIG. 4. (Color online) Same "horizontal cut" as Fig. 3 except at commensurate density for the boson species alone $\rho_B=1$ and $\rho_F=1/4$. Top panel: The bosons are insulating at weak U_{BF} within this Mott lobe of commensurate bosonic filling (region IV of the phase diagram). However, the fermions are free to flow on the uniform boson background and have nonzero stiffness. Upon emerging from the lobe, at $U_{BF} \approx 2U_{BB}$, ρ_B^s becomes nonzero in a window where the two repulsions work against each other. After the peak, the system becomes phase separated and ρ_B^s and ρ_F^s go to zero. Bottom panel: The correlated and anticorrelated stiffnesses are essentially equal throughout the weak coupling because the flow is dominated by fermions. However, in the window the anticorrelated stiffness increases beyond the correlated stiffness in a weak simulacrum of phase II (as discussed in the text).

dow opens for both species. Finally, for $U_{BF}>2U_{BB}$, it is energetically unfavorable for a boson to share a site with a fermion. We enter a region of phase separation where superflow for both species stops, but the compressibilities κ_B and κ_F are nonzero. We also confirm phase separation through a density structure factor. See also [13,17].

VI. SUPERFLUID RESPONSE AT GENERAL FILLING

Further insight into the physics of this phase diagram can be obtained by measuring the superfluid response along the same "vertical" cuts through the phase diagram as done in Figs. 1 and 2, in which ρ_B is varied at fixed U_{BF}. In Figs. 5 and 6, we show the result. Distinctive densities in the latter figures are $\rho_B=3/4$ (so that $\rho_B+\rho_F=1$) and $\rho_B=1$. We discuss first (Fig. 5) the case of $U_{BF}=16$, where increasing ρ_B cuts through both Mott lobes. The bosonic superfluid density vanishes at $\rho_B=1$, dips at $\rho_B+\rho_F=1$, and is nonzero above, below, and between the lobes. The fermion superfluid density is
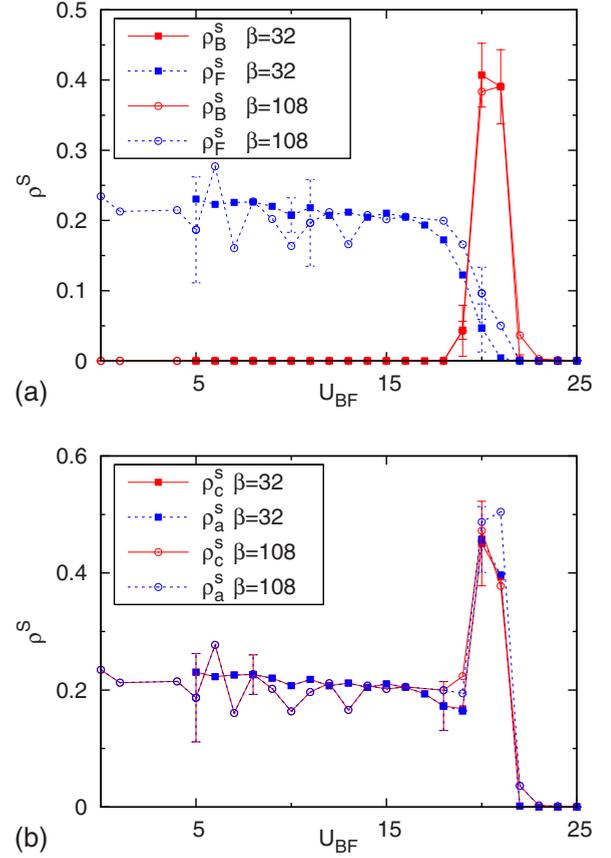
never driven to zero in this cut, and only dips at the special value $\rho_B=3/4$ where the commensurate total density works against superfluidity. In the case of $U_{BF}=24$, Fig. 6, as ρ_B increases we cut through only the $\rho_B=3/4$ lobe. Here the superfluid density is pushed to zero for the entire region between $\rho_B=3/4$ and $\rho_B=1$, and is nonzero without.

We now fill in the labeling of the phase diagram of Fig. 2. A gapless superfluid phase (I) with ($\rho_B^s \neq 0$ and $\rho_F^s \neq 0$) exists at low filling of the lattice $\rho_B+\rho_F<1$. When the combined filling of the two species becomes commensurate, an anticorrelated (II) phase appears in which $\rho_B^s \neq 0$ and $\rho_F^s \neq 0$, but $\rho_B^s=\rho_F^s$. This phase is characterized by superflow of the two species in opposite directions and is gapped to the addition of bosons or fermions. The usual bosonic Mott insulator, phase IV, occurs at commensurate boson densities. However, it can be melted by increasing U_{BF} since the jump in bosonic
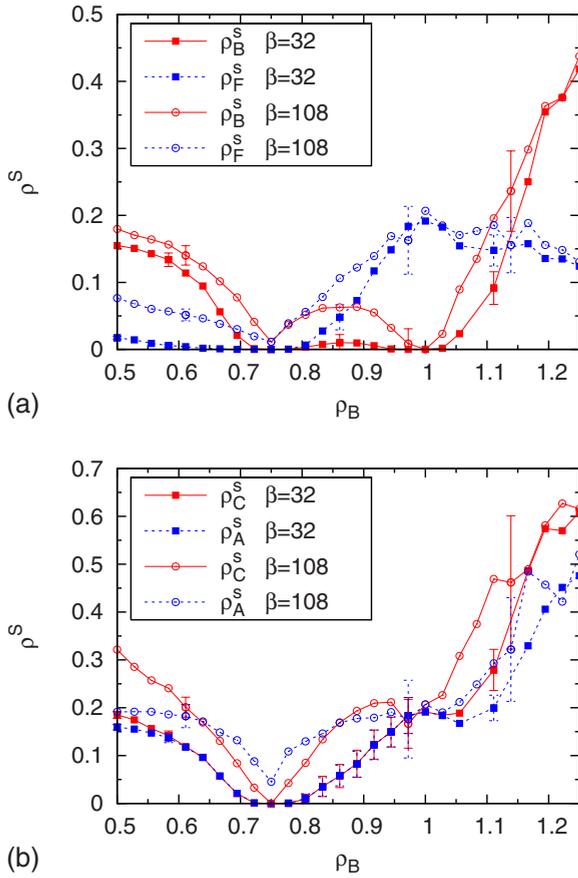
FIG. 5. (Color online) "Vertical" sweep across ρ_B at $\rho_F=1/4$, $U_{BB}=10$, and $U_{BF}=16$. Top panel: The boson superfluid density changes much less as β is increased from $\beta=32$ to $\beta=108$ in the superfluid phase I at $\rho_B<3/4$ and $\rho_B>1$ than for phase III $3/4<\rho_B<1$. This is a hallmark of the "relay" superfluid discussed in the text. Bottom panel: The correlated winding decreases to zero at $\rho_B=3/4$ while the anticorrelated winding remains finite. As ρ_B is increased beyond $3/4$ the correlated winding increases and overtakes the anticorrelated winding. This is another sign of the relay superfluid.

chemical potential (Mott gap) is reduced to $2U_{BB}-U_{BF}$. There is no jump in μ_F. Eventually quantum fluctuations break this gap and superflow is allowed. When U_{BF} exceeds $2U_{BB}$, all superflow stops and we enter the insulating region V of the phase diagram.

We speculate that the nature of the superfluidity in the narrow phase III, which exists between the two Mott lobes is an unusual "relay" process. It is similar to the usual superfluid which exists between Mott lobes in the single species model, in that $\rho_B^s \neq 0$. However, the temperature scale at which superfluid correlations build up is dramatically reduced. This occurs because the bosons can exhibit superflow only by traveling along with a fermion partner, and being handed off from fermion to fermion in order to wind around the entire lattice. The point is that because $2U_{BB}$ exceeds U_{BF} the bosons doped into the lattice above $\rho_B=1-\rho_F=3/4$ are forced to sit on a fermion. They cannot hop off, but the fermion can move since it has already paid U_{BF} to share a site with a boson. Now, the fermions cannot pass each other once a fermion riding atop bosons runs into a fermion alone
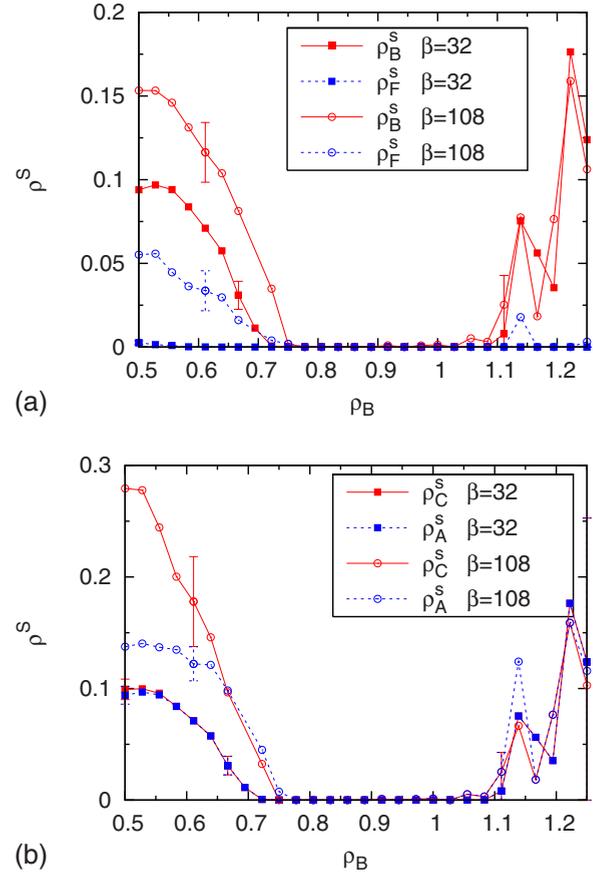

FIG. 6. (Color online) Vertical sweep across ρ_B at $\rho_F=1/4$, $U_{BB}=10$, and $U_{BF}=24$. Unlike the case for the weaker coupling $U_{BF}=16$ in Fig. 5, both superfluid densities vanish in the insulating region of the Mott lobe at commensurate total filling.

on a site. The fermion without a boson cannot move out of the other fermion's way either. However, the boson sharing a site with the mobile fermion can then hop to the immobile fermion at no energy cost. Thus, the boson is passed from one fermion to the other, granting it mobility. Signatures of this phase are the lower value of the temperature at which the superfluid density builds up, that $\rho_F^s > \rho_B^s$, and more correlated winding than anticorrelated. However, there is nothing preventing lone fermions from acting as in the anticorrelated superfluid phase. Unfortunately this means that potential signals are masked. While we do see some of these signatures (Fig. 5) in the specified region, the numbers are not completely conclusive and will require further investigation.

VII. MOMENTUM DISTRIBUTION FUNCTIONS

To further explore the nature of the phases we turn to the momentum distributions for the bosons, fermions, and anticorrelated pairing—Figs. 7–12. Each plot is made at $\beta=108$ and corresponds to the parameter choices: I, $U_{BF}=16$ and $N_B=20$; II, $U_{BF}=16$ and $N_B=27$; III, $U_{BF}=16$ and $N_B=32$; IV, $U_{BF}=16$ and $N_B=36$; V, $U_{BF}=30$ and $N_B=27$; VI, $U_{BF}=28$ and $N_B=36$. In the superfluid phase (I), there is a peak in the boson distribution and a plateau in the fermion distribution, implying quasicondensation in the bosonic sec-
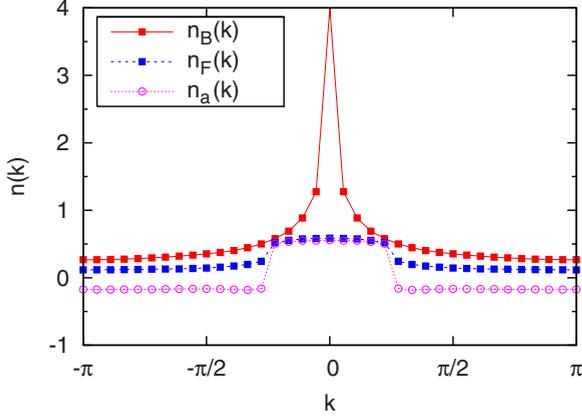
FIG. 7. (Color online) I, $U_{BF}=16$, $U_{BB}=10$, $\beta=108$, and $N_B=20$; momentum distributions for bosons and fermions, and Fourier transform of the anticorrelated pairing [$n_a(k)$] Green function. The sharp peak in bosonic momentum distribution indicates the presence of a quasicondensate, while fermions have a plateau indicating Luttinger liquidlike behavior with a clear Fermi momentum, a property that is also shared by the composite fermions described by the anticorrelated pairing.

FIG. 9. (Color online) III, $U_{BF}=16$, $U_{BB}=10$, $\beta=108$, and $N_B=32$. Qualitatively, this picture is similar to Fig. 7—we have a peak in the bosonic momentum distribution and a plateau in the fermionic and anticorrelated pairing momentum distributions, all indicating power-law decaying correlations of their corresponding real space Green functions.

tor and Luttinger liquidlike behavior in the fermionic one. In the anticorrelated phase (II) there is neither of the former behaviors, but the Fourier transform of the anticorrelated pairing Green function has a clear Fermi momentum showing Luttinger-type physics of the composite fermions (formed by pairing a fermion and a boson) [11,24]. The relay superfluid phase (III) displays momentum distributions that are similar to the ones of superfluid phase (I). Next, in the Mott-insulator/Luttinger liquid phase (IV) one can see a clear Fermi momentum in the bare fermion $n_F(k)$ and a very smooth behavior of $n_B(k)$ and $n_a(k)$, which show that their real space Green function counterparts are decaying exponentially. In the insulating phase (V) all the correlations decay exponentially and their corresponding momentum distri-
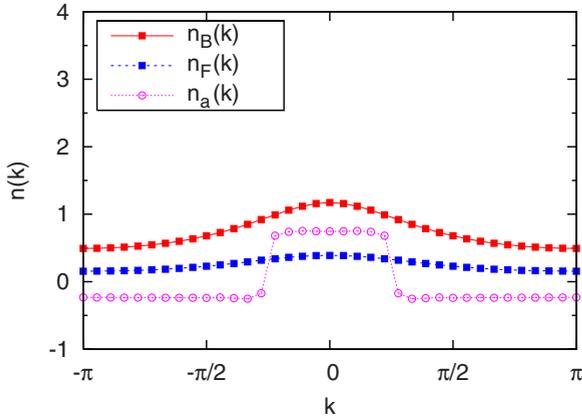
bution functions are smooth functions of k. In the case of phase separation (VI) the bosonic momentum distribution is similar to the superfluid, while fermionic distribution is similar to that of an insulator.

VIII. CONNECTION TO PREVIOUS THEORETICAL WORK

As reviewed in the Introduction, there is extensive theoretical literature on Bose-Fermi mixtures. We now make more detailed contact with previous work, first by comparing our results to the strong coupling phase diagram of Lewenstein *et al.* (LSBF) [8]. Figure 13 combines our results and those of LSBF. Besides the quantitative agreement, we note the following correspondences: LSBF's region $0 \leq \bar{\mu} \leq 1$ is analogous to our $0 \leq \mu \leq 20$, and $0 \leq \alpha \leq 1$ to our $0 \leq U_{BF} \leq 20$. Furthermore, our phase II (anticorrelated phase) corre-

FIG. 8. (Color online) II, $U_{BF}=16$, $U_{BB}=10$, $\beta=108$, and $N_B=27$. Bosons do not have a peak at $k=0$ and the Fermi momentum is washed out, both reflecting the onset of short range one-particle correlations. On the other hand, the plateau in the Fourier transform of the anticorrelated pairing shows that the composite fermions formed by pairing a fermion and a boson have a well defined Fermi momentum [11].
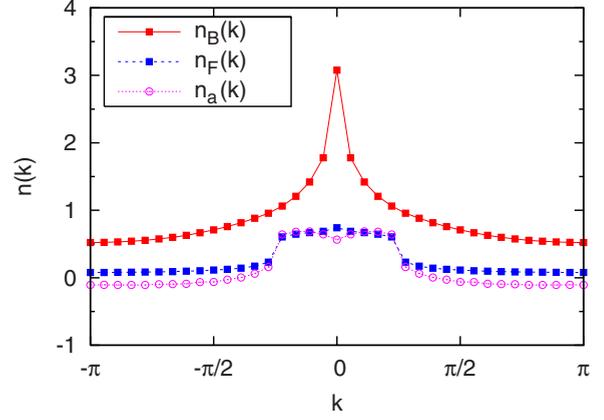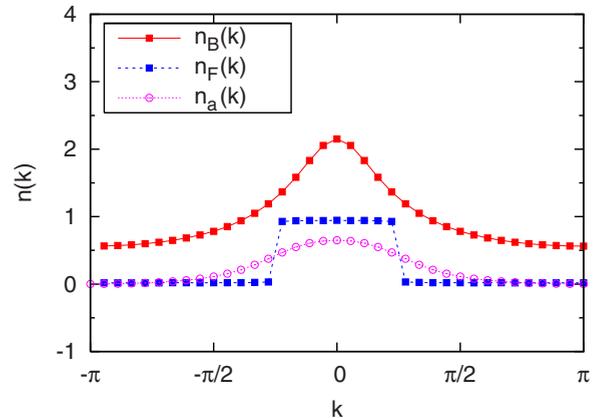

FIG. 10. (Color online) IV, $U_{BF}=16$, $U_{BB}=10$, $\beta=108$, and $N_B=36$. There is no sharp peak in $n_B(k)$ and a plateau in $n_F(k)$ is present. This phase is a Mott insulator for bosons and Luttinger liquid behavior for the fermions. In this case the composite fermions do not exhibit a Fermi momentum.
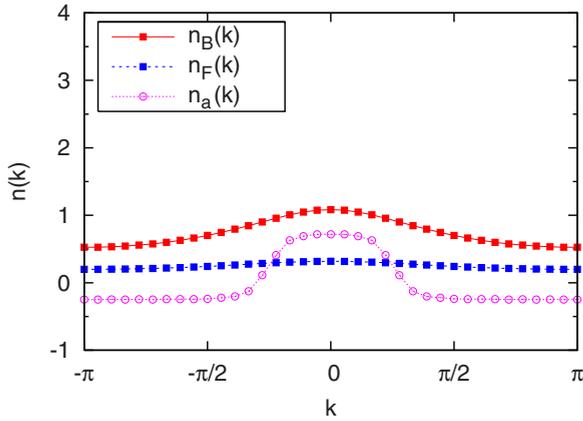
FIG. 11. (Color online) V, $U_{BF}=30$, $U_{BB}=10$, $\beta=108$, and $N_B=27$. The momentum distribution functions in this case exhibit the behavior expected from an insulator, i.e., no sharp peak in $n_B(k)$, no plateau in $n_F(k)$, and no Fermi edge in $n_a(k)$.

sponds to LSBF's phase $\overline{\mathrm{II}}_{FL}$ (Fermi liquid of composite fermions formed by one bare fermion and bosonic hole); our phase IV (Mott insulator/Luttinger liquid) to LSBF's phase I_{FL} (Fermi liquid); and finally, our phase III (anticorrelated phase/relay superfluid) to LSBF's phase I_{DW} (density wave phase). These three phases have similar qualities and occur approximately at the same locations at our and LSBF's phase diagrams.

Both calculations suggest the existence of composite particles. Our phase V (insulator) corresponds to LSBF's phase $\overline{\mathrm{II}}_{FD}$, a region of fermionic domains of composite fermions formed by one bare fermion and bosonic hole. There is one case when the phases do not seem to correspond well, namely, LSBF's phase $\overline{\mathrm{II}}_{SF}$ which is a superfluid of composite fermions formed by one bare fermion and bosonic hole. Our results (Fig. 3) instead suggest that in this region of $U_{BF}>2U_{BB}$, the superfluid densities vanish, or are very small.
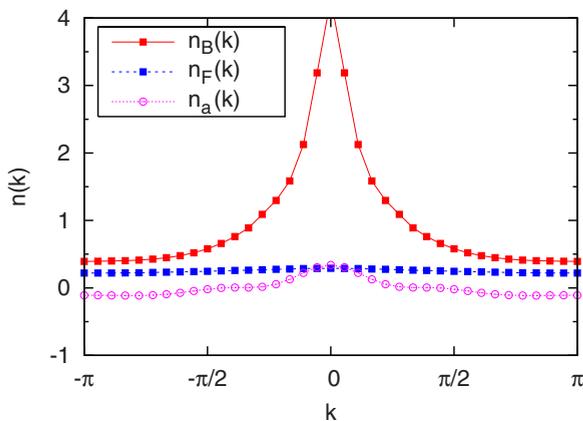

FIG. 12. (Color online) VI, $U_{BF}=28$, $U_{BB}=10$, $\beta=108$, and $N_B=36$. This is phase separation. The boson momentum distribution function has a peak indicating that there may be a kind of superflow in their separate area. Fermions, on the other hand, behave as an insulator. The $n_a(k)$ curve indicates that the coupling between bosons and fermions is weak, as we would expect in phase separation.
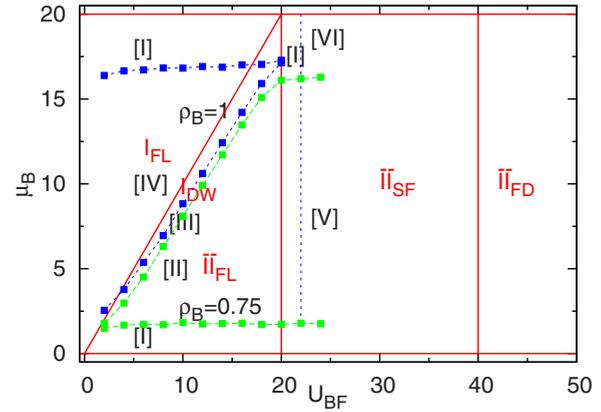

FIG. 13. (Color online) A comparison of our phase diagram (Fig. 2) with the strong coupling boundaries. Symbols and dashed lines are the results of the present QMC work, while the solid lines are for $t_B=t_F=0$. Unsubscripted Roman symbols denote our phases while subscripted Roman symbols are the labeling of Lewenstein *et al.* [8].

IX. EXPERIMENTAL ISSUES

Albus *et al.* [14] have given the correspondence between Hubbard model parameters U_{BB}, U_{BF}, t_B, t_F and experimentally controlled parameters. U_{BB} and U_{BF} are determined by the optical lattice depth, laser wavelength, and harmonic oscillator lengths, as well as by the scattering lengths a_{BB} and a_{BF}, which can be tuned by traversing a Feshbach resonance. Similarly, the hoppings t_B and t_F follow from the lattice depth and atomic masses. It is possible to choose experimentally reasonable values of these parameters to correspond to the energy scales chosen in our paper. For example, following Albus *et al.*, for a ^{87}Rb, ^{40}K mixture and laser wavelength 600 nm, $a_{BB}=100a_0$, $a_{BF}=123.74a_0$, and $V_0=0.7614$ in units of boson recoil energy, with $l_B^\perp=17.04$ nm, we get in units of t_B: $t_B=1$, $t_F=2$, and $U_{BB}=U_{BF}=10$. In this paper we have used $t_B=t_F=1$, which would be accessible in mixtures with $m_F\approx m_B$ such as ^{40}K, ^{41}K.

X. CONCLUSIONS

In conclusion, we have mapped out the boson density-interaction strength phase diagram of Bose-Fermi mixtures. The Mott lobe at commensurate total density has nontrivial superfluid properties, where the two components of superflow can be nonzero and anticorrelated, or both vanish. Likewise the Mott lobe at commensurate bosonic density has vanishing boson superflow and nonzero fermion stiffness. ρ_B^s is nonzero upon emerging from this lobe where the balance between boson-boson and boson-fermion repulsions opens a superfluid window, with anticorrelated superflow. The superfluidity between the two Mott regions may be of a different type where the bosons travel along with the fermions (chosen to have relatively low density in this work). As a consequence, the superfluid onset temperature is significantly reduced. Finally, we have discussed the signatures of the above phases in the momentum distribution function of fermions and bosons, which can be measured in time of flight experiments.

[1] M. Greiner, O. Mandel, T. Esslinger, T. W. Hänsch, and I. Bloch, Nature (London) **415**, 39 (2002).

[2] D. Jaksch, C. Bruder, J. I. Cirac, C. W. Gardiner, and P. Zoller, Phys. Rev. Lett. **81**, 3108 (1998).

[3] H. Ott, E. de Mirandes, F. Ferlaino, G. Roati, G. Modugno, and M. Inguscio, Phys. Rev. Lett. **92**, 160601 (2004).

[4] K. Günter, T. Stöferle, H. Moritz, M. Köhl, and T. Esslinger, Phys. Rev. Lett. **96**, 180402 (2006).

[5] S. Ospelkaus, C. Ospelkaus, L. Humbert, K. Sengstock, and K. Bongs, Phys. Rev. Lett. **97**, 120403 (2006).

[6] M. Zaccanti, C. D'Errico, F. Ferlaino, G. Roati, M. Inguscio, and G. Modugno, Phys. Rev. A **74**, 041605(R) (2006).

[7] M. A. Cazalilla and A. F. Ho, Phys. Rev. Lett. **91**, 150403 (2003).

[8] M. Lewenstein, L. Santos, M. A. Baranov, and H. Fehrmann, Phys. Rev. Lett. **92**, 050401 (2004).

[9] L. Mathey, D.-W. Wang, W. Hofstetter, M. D. Lukin, and E. Demler, Phys. Rev. Lett. **93**, 120404 (2004); L. Mathey and D.-W. Wang, Phys. Rev. A **75**, 013612 (2007).

[10] A. Imambekov and E. Demler, Phys. Rev. A **73**, 021602(R) (2006).

[11] L. Pollet, M. Troyer, K. Van Houcke, and S. M. A. Rombouts, Phys. Rev. Lett. **96**, 190402 (2006).

[12] P. Sengupta and L. P. Pryadko, Phys. Rev. B **75**, 132507 (2007).

[13] F. Hébert, F. Haudin, L. Pollet, and G. G. Batrouni, Phys. Rev. A **76**, 043619 (2007).

[14] A. Albus, F. Illuminati, and J. Eisert, Phys. Rev. A **68**, 023606 (2003).

[15] M. Cramer, J. Eisert, and F. Illuminati, Phys. Rev. Lett. **93**, 190405 (2004).

[16] L. Pollet, C. Kollath, U. Schollwöck, and M. Troyer, Phys. Rev. A **77**, 023608 (2008).

[17] A. Mering and M. Fleischhauer, Phys. Rev. A **77**, 023601 (2008).

[18] V. G. Rousseau and P. J. H. Denteneer, Phys. Rev. A **77**, 013609 (2008).

[19] M. P. A. Fisher, P. B. Weichman, G. Grinstein, and D. S. Fisher, Phys. Rev. B **40**, 546 (1989).

[20] K. Van Houcke, S. M. A. Rombouts, and L. Pollet, Phys. Rev. E **73**, 056703 (2006).

[21] S. M. A. Rombouts, K. Van Houcke, and L. Pollet, Phys. Rev. Lett. **96**, 180603 (2006).

[22] G. G. Batrouni, R. T. Scalettar, and G. T. Zimanyi, Phys. Rev. Lett. **65**, 1765 (1990).

[23] N. V. Prokof'ev, B. V. Svistunov, and I. S. Tupitsyn, JETP **87**, 310 (1998).

[24] Unlike $n_B(k) = \langle \psi_0 | b^\dagger(k) b(k) | \psi_0 \rangle$, which is the length of a vector and hence must be positive, there is no such constraint on $n_a(k)$, which is the Fourier transform of $G_{ij}^a = \langle b_i^\dagger b_j f_j^\dagger f_i \rangle$. We have verified that the same small negative values of $n_a(k)$ in the figures are also obtained in exact diagonalization on small clusters.

[25] This phase has been termed "super-Mott" as a consequence of its combining a nonzero gap with nonzero superflow [18].